Journal of *Marine Science and Engineering*

MDPI

Article

Experimental and Numerical Study on Trajectory Tracking of Remotely Operated Vehicles Involved in Cleaning Aquaculture Vessels

Hua Zhang [1,2], Shuangxi Xu [1,*] and Yonghe Xie [2,*]

[1] School of Naval Architecture, Ocean and Energy Power Engineering, Wuhan University of Technology, Wuhan 430070, China; gongchengzhh@zjou.edu.cn
[2] School of Naval Architecture and Maritime, Zhejiang Ocean University, Zhoushan 316022, China
* Correspondence: xushuangxi19832@163.com (S.X.); xieyh@zjou.edu.cn (Y.X.)

Abstract: Efficient cleaning is crucial in aquaculture vessels; however, Remotely Operated Vehicles (ROVs) encounter difficulties in regard to trajectory tracking within confined chambers, because of structural nonlinearities and environmental disturbances. To address these challenges, this paper proposes a multi-scale dynamic sliding mode adaptive control (MDSMAC) scheme to compensate for the effects of structural nonlinearities and external disturbances, achieving precise trajectory tracking. Based on a six-degree-of-freedom motion model, an adaptive multi-scale sliding mode control mechanism is designed, enabling the system to adapt to scale variations and environmental disturbances, enhancing control accuracy and robustness. The asymptotic stability of the system is rigorously proven using the second Lyapunov method. The numerical simulation results show that the proposed method exhibits superior robustness to external disturbances and high precision in complex environments, confirming its long-term stability. Water tank experiments were conducted to further evaluate the trajectory tracking performance of the method under nonlinear system control. The results show the high level of feasibility and strong potential of the approach for practical applications.

Keywords: remotely operated vehicle; multi-scale sliding mode control; trajectory tracking; nonlinear system control; aquaculture vessels

Academic Editor: Sergei Chernyi

Received: 2 December 2024
Revised: 24 December 2024
Accepted: 24 December 2024
Published: 31 December 2024

Citation: Zhang, H.; Xu, S.; Xie, Y. Experimental and Numerical Study on Trajectory Tracking of Remotely Operated Vehicles Involved in Cleaning Aquaculture Vessels. *J. Mar. Sci. Eng.* **2025**, *13*, 56. https://doi.org/10.3390/jmse13010056

1. Introduction

Biofouling significantly degrades water quality in marine aquaculture. This affects aquaculture product yield, leading to annual economic losses of approximately USD 1.5 to USD 3 billion [1,2]. The design of underwater cleaning robots that can enhance economic efficiency is of great significance. The precise six-degree-of-freedom (6-DOF) trajectory tracking of Remotely Operated Vehicles has substantial research value. ROVs are widely used in fields such as military reconnaissance and marine aquaculture, significantly improving operational safety and efficiency, particularly in hazardous or inaccessible environments [3,4]. As the complexity of the operational environment increases, ROV control systems face significant challenges in dealing with structural nonlinearities, external disturbances, and spatial constraints. These factors not only exacerbate system uncertainties, but also impose higher demands on real-time trajectory tracking [3]. Developing advanced control strategies that effectively manage system nonlinearities and external disturbances has become crucial.

In the field of ROV control, several methods have been proposed to handle uncertainties and external disturbances. These include traditional control approaches like Proportional–Integral–Derivative (PID) control [5,6] and more advanced techniques such as Fuzzy Logic Control (FLC) [7], sliding mode control (SMC) [8], Model Predictive Control (MPC) [9,10], and neural network control (NNC) [11,12]. Each approach presents distinct advantages in specific scenarios; however, these approaches also encounter inherent limitations when applied in the dynamic and nonlinear marine environment.

Although PID control is widely employed due to its simplicity and ease of implementation, its performance is constrained in regard to dynamic systems and when subject to significant external disturbances. Research has shown that PID control can effectively regulate ROV motion over short durations. For instance, a study utilizing Simulink simulations demonstrated PID's effectiveness in controlling surge, heave, and yaw, maintaining stability at a set position for approximately 3 to 4 s [5]. However, when faced with the nonlinearities and substantial disturbances characteristic of marine environments, PID control performs inadequately in terms of long-duration trajectory tracking, failing to sustain precise control. Thus, while PID control proves effective in certain scenarios, its adaptability and robustness in complex marine environments are notably limited.

FLC offers advantages in handling uncertainty and nonlinearities. but also presents notable limitations. Primarily, its reliance on manually defined fuzzy rules reduces its adaptability in dynamic and complex environments. Although combining PID with fuzzy control can improve the precision and response speed through FPGA implementation [7], issues of computational complexity and real-time performance remain, particularly during long-duration operations in complex settings. While studies suggest that FLC can enhance control accuracy and reduce the response time, its robustness and stability when subject to strong nonlinearities and large disturbances still require improvement. Thus, while FLC performs effectively in regard to certain tasks, its limitations must be addressed for optimized performance in complex underwater environments.

SMC exhibits significant advantages in regard to underwater robot control, particularly due to its robustness in addressing system uncertainties and external disturbances [8]. However, SMC also has some inherent limitations. Firstly, SMC is prone to causing "chattering" phenomena, especially when approaching the sliding surface, where the system may experience high-frequency oscillations that adversely affect control precision and system smoothness. Although higher-order sliding mode control and adaptive control techniques can alleviate this issue to some extent, completely eliminating chattering remains a challenge in complex underwater environments. While the computational complexity of sliding mode control is typically low, certain applications, such as higher-order or adaptive sliding mode control, significantly increase the computational demands. In real-time underwater robot control, these increased computational requirements may pose challenges to hardware resources, thereby limiting its applicability in regard to embedded systems. Therefore, although sliding mode control offers excellent robustness, further optimization is required to reduce the computational complexity and improve its stability and real-time performance in complex underwater environments.

MPC offers significant advantages in regard to underwater robot control, particularly in effectively handling complex constraints and optimizing trajectory tracking in dynamic environments [9,10]. By predicting future states and adjusting control inputs in real time, MPC minimizes trajectory errors, making it especially suitable for high-dimensional and multivariable control systems. However, the primary limitation of MPC lies in its high computational complexity. Each sampling period requires an optimal control problem to be solved, which demands considerable computational resources and may lead to response delays, especially in real-time applications. Underwater robots often operate in complex

environments where real-time performance is crucial, presenting challenges for applying MPC in hardware with limited computational capacity. Additionally, MPC relies on precise system models, but the dynamic characteristics of underwater robots are complex and are influenced by environmental factors, meaning modeling errors could limit its practical performance. Therefore, while MPC theoretically offers powerful optimization capabilities, its computational complexity and reliance on model accuracy remain significant bottlenecks for its application in underwater robot control [13].

NNC demonstrates strong adaptability in regard to underwater robot control, effectively addressing complex nonlinear dynamics and external disturbances [11,12]. However, the application of NNC also presents certain limitations. Firstly, the training process of neural networks requires a large amount of high-quality data, and the complexity and dynamic nature of the underwater environment make data collection a significant challenge. Secondly, the performance of NNC is highly dependent on the optimization of the network structure and parameters, a process that typically involves repeated trials and adjustments, thereby increasing the design complexity and computational burden. Lastly, although neural networks can enhance system robustness, their high computational demands may still impact real-time performance, particularly in embedded systems with limited resources. Therefore, while neural network control holds potential advantages, its widespread application in underwater robots faces challenges related to data requirements, model optimization, and computational efficiency.

In recent years, sliding mode control has been widely applied in nonlinear systems due to its robustness. Miao Y. proposed a Recurrent Fuzzy Sliding Mode Control (RF-SMC) method, which combines fuzzy logic with neural networks to manage multi-scale disturbances effectively and improve system adaptability [14]. Among intelligent control strategies, Chengqi L. developed a Kalman filter-based MPC approach that successfully compensated for external disturbances in ROV trajectory tracking [15]. However, the high computational complexity of MPC limits its broader application in regard to real-time control. Xu Z. introduced an adaptive non-singular integral terminal sliding mode control method, which addresses uncertainties in dynamic models and external disturbances, particularly excelling in achieving fast convergence [16].

These methods have made significant progress in handling uncertainties and external disturbances, but challenges persist in addressing complex disturbances [17,18]. Particularly, the highly dynamic and nonlinear nature of marine environments adds to the complexity, making it difficult for existing control methods to maintain precision and robustness in the presence of multi-scale disturbances. Designing control strategies that can effectively manage multi-scale disturbances in complex marine environments is crucial for improving ROV trajectory tracking performance.

In response to the trajectory tracking challenges posed by structural nonlinearities, parameter uncertainties, external environmental disturbances, and strong disturbances during operational tasks involving underwater aquaculture cleaning, this paper proposes a multi-scale dynamic sliding mode adaptive control (MDSMAC) mechanism, which integrates multi-scale sliding mode surface design with an adaptive control strategy to effectively address the trajectory tracking challenges posed by system nonlinearities, parameter uncertainties, and strong disturbances in regard to underwater ROV cleaning tasks in marine environment. MDSMAC innovatively uses a saturation function to mitigate the common issue of chattering in sliding mode control, and by adopting a multi-scale scheme, the sliding mode surface is controlled using different dynamic parameters for large-scale and small-scale states, achieving more precise control. The system is equipped with an adaptive strategy that automatically tracks external disturbances and adjusts the control parameters in real time to adapt to changes in the external environment. This method not only

dynamically adapts to multi-scale variations in the external environment, but also provides precise compensation for short-term fluctuations and long-term uncertainties, ensuring stable and efficient operation in complex and dynamic marine conditions. MDSMAC shows superior performance in handling highly nonlinear systems and is ideal for underwater cleaning, inspection tasks, significantly improving the trajectory tracking performance and ensuring long-term stability, even in the presence of strong external disturbances and multiple uncertainties.

2. Modeling and Theoretical Framework

2.1. Dynamic Model of ROVs in Marine Environments

To derive the equations of motion for marine vessels, it is essential to study rigid body motion, hydrodynamics, and hydrostatics. We use the Newton–Euler formulation and vector mechanics to derive the rigid-body equations of motion. Based on Fossen's underwater vehicle model, the 6-DOF model of ROVs accounts for nonlinearities in the structure, considering parameter uncertainties and coupling effects between fluids and solids, which are typically represented by added mass and nonlinear damping terms. In addition, the mass of the ROV, fluid drag coefficients, and other model parameters may vary dynamically in different ocean environments, further increasing the uncertainty of the model. External disturbances, such as ocean currents and waves, add complexity due to their randomness and the difficulty in achieving precise modeling. To address these challenges, external disturbances and parameter uncertainties are treated as dynamic disturbance terms and are compensated for in real time through adaptive control strategies, ensuring that the ROV maintains stable trajectory control, even in complex marine environments. The dynamic equation of the ROV can be expressed as shown in Equation (1) [3,16]:

$$M\dot{\nu} + C(\nu)\nu + D(\nu)\nu + g(\eta) = \tau + \tau_d \tag{1}$$

where M represents the inertia matrix, which includes the ROV's mass and added mass; $C(\nu)$ is the Coriolis and centripetal matrix, consisting of both the rigid body and added mass components. It depends on the ROV's rotational velocity. Moreover, $D(\upsilon)$ denotes the damping matrix, representing linear and nonlinear hydrodynamic damping forces. Linear damping accounts for drag proportional to the velocity, while nonlinear damping includes turbulence and vortex shedding effects. In addition, $g(\eta)$ represents the restoring forces and moments due to buoyancy and gravity, where η is the position and orientation vector [17,18]. Then, τ is the control input, representing forces generated by the thrusters. Where τ_d is the external disturbance, including ocean currents and waves. The restoring forces are represented by the buoyancy force, B, and the weight of the ROV, W, where $B > W$ ensures a positive buoyancy.

The fluid resistance of the ROV in water is described by the linear and nonlinear damping coefficients. The nonlinear damping terms primarily reflect turbulence in the boundary layers and vortex-induced shedding. External disturbances, such as ocean currents, are modeled as random processes, often assumed to follow a Gaussian distribution for simplicity [19–21].

2.2. Control Objectives and Thruster Configuration Design

The ROV's propeller configuration consists of three sets of thrusters arranged perpendicularly along the X(T1–T4), Z(T5–T6), and Y(T7–T8) axes, forming a symmetrical layout as shown in Figure 1. This design minimizes the interference between thrusters, ensuring stable control of the ROV's motion in highly dynamic environments. The arrangement of

the thrusters is carefully designed to handle multidirectional coupling effects, especially during complex attitude control, allowing precise maneuverability.

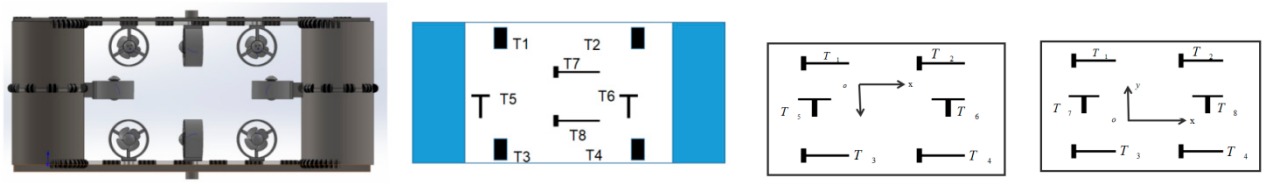

Figure 1. Structure diagram of the ROV, thruster layout, and power distribution.

The symmetrical layout enhances the ROV's stability and agility in challenging marine environments. By optimizing the positioning of the thrusters, the ROV can reduce thrust loss during sharp turns, vertical movement, or lateral drifting, improving the overall efficiency of the system. Each set of thrusters includes a pair of forward and reverse propellers, with the thrust direction and magnitude controlled by the modulating voltage and current inputs. This allows for 6-DOF control, enabling the ROV to maintain stable thrust output, even in challenging ocean conditions. The real-time adjustment of these inputs helps the system adapt to dynamic ocean conditions, compensating for external disturbances and maintaining system stability and safety.

To optimize the power distribution, a control allocation matrix maps the input control vector to the corresponding thrust output of each propeller. Based on the manufacturer's datasheet, the thrust of each propeller is a function of the applied voltage and current, which are dynamically adjusted in real time according to the control demands. The thrust matrix is expressed in Equation (2):

$$T_{matrix} = \begin{bmatrix} X \\ Y \\ Z \\ K \\ M \\ N \end{bmatrix} = \begin{bmatrix} 1 & 1 & 1 & 1 & 0 & 0 & 0 & 0 \\ 0 & 0 & 0 & 0 & 0 & 0 & 1 & 1 \\ 0 & 0 & 0 & 0 & 1 & 1 & 0 & 0 \\ l_1 & l_2 & l_3 & l_4 & 0 & 0 & 0 & 0 \\ 0 & 0 & 0 & 0 & 0 & 0 & l_7 & l_8 \\ 0 & 0 & 0 & 0 & l_5 & l_6 & 0 & 0 \end{bmatrix} \begin{bmatrix} f_1 \\ f_2 \\ f_3 \\ f_4 \\ f_5 \\ f_6 \\ f_7 \\ f_8 \end{bmatrix} = Bu \tag{2}$$

This matrix captures the relationship between the control input vector and the output forces from the thrusters, ensuring efficient power usage. By dynamically adjusting the thrust for each axis, the system maintains accurate trajectory tracking and ensures stability, even under varying disturbance conditions.

2.3. Kinematic Modeling and Reference Frame Analysis

The ROV motion control system is inherently nonlinear and subject to uncertainties. The coordinate systems used are depicted in Figure 2, which shows both the inertial $E(\xi, \eta, \zeta)$ and body-fixed coordinate systems $O(x, y, z)$. These two systems are essential for describing the posture of the ROV, where the inertial coordinate system is used for the global reference and the body-fixed system tracks the ROV's orientation and movement. The positions of the ROV are represented by x, y, z, while the Euler angles, relative to the inertial coordinate system, are denoted by φ, θ, ψ. The variables $\dot{x}, \dot{y}, \dot{z}$ represent the rates of change in the ROV's position relative to the inertial coordinate system. The variables φ, θ, ψ indicate the rates of change of the Euler angles of the ROV relative to the inertial coordinate system. The variables u, v, w denote the linear velocities in terms of

the moving coordinate system. The angular velocities of the ROV relative to the moving coordinate system are represented by p, q, r, respectively [3,5,22].

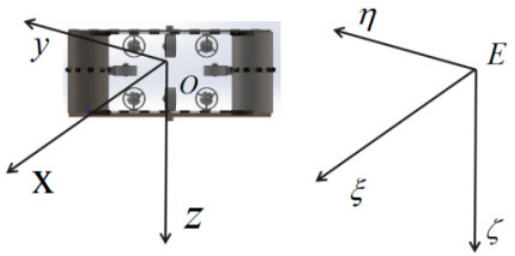

Figure 2. The two reference frames.

The kinematic behavior of the six-degree-of-freedom ROV can be expressed using two reference frames: the North–East–Down (NED) reference frame and the body-fixed reference frame. The transformation between these two frames can be expressed as Equation (3):

$$\eta = J(\dot{\eta})\nu \tag{3}$$

where $\dot{\eta}$ represents the velocities in the inertial frame; ν denotes the velocities in the body-fixed frame; $J(\eta)$ is the transformation matrix dependent on the Euler angles.

The 6-DOF motion model of the ROV is defined by its complex dynamic interactions between fluid forces and its rigid body. This model reflects the ROV's nonlinear dynamics and the parameter uncertainties arising from the changing ocean environment. These nonlinear dynamics need to be managed by the control system, ensuring accurate trajectory control despite external disturbances, such as waves and currents.

2.4. Multi-Scale Sliding Mode Control Strategy

The sliding mode control strategy is widely used to handle nonlinear systems and external disturbances. However, in complex marine environments, the intensity and frequency of unknown disturbances can change, leading to significant uncertainty in the system parameters of nonlinear robotic systems. Single-scale sliding mode control often struggles to balance system robustness and control precision when subject to varying conditions. Larger parameter variations require stronger control actions to enhance system robustness, while smaller parameter variations demand finer adjustments to avoid instability due to over control. To address this issue, this paper proposes a multi-scale sliding mode control strategy. By designing sliding surfaces at different scales, the system can dynamically balance robustness and precision when faced with varying levels of disturbances and parameter changes.

According to Equation (1), the nonlinear system can be reformulated as in Equation (4):

$$\begin{cases} \dot{x}_1 = x_2 \\ \dot{x}_2 = p_1(x,t) + p_2(x,t) + p_3(x,t) \end{cases} \tag{4}$$

where $p_1(x,t) = P_M(C_\nu(\nu)\nu + D_\nu(\nu)\nu + g(\eta))$, $p_2(x,t) = P_M\tau_f$, $p_3(x,t) = P_M(\Delta f + \tau_d)$ $= P_M(M_A\dot{x} + C_A(\nu)x + D_N(\nu)x + g(\eta) + \tau_d)$ and $P_M = -M^{-1}$. Where p_1 represents the system's dynamic characteristics in a linear state. It includes the inertia matrix M, Coriolis matrix $C(\nu)$, and damping matrix $D(\nu)$. These matrices describe the system's inertial properties, the Coriolis effects, and linear damping behavior under ideal conditions, reflecting the fundamental dynamics of the system. In addition, p_2 represents the system's controlled state under external forces. This part describes how external forces influence the system's state in the absence of disturbances and nonlinear effects, illustrating how

external inputs affect the motion of the robot through the dynamic system. Moreover, p_3 accounts for the effects of nonlinearities and external disturbances on the system's state. It includes the added mass matrix M_A, added Coriolis matrix $C_A(\nu)$, nonlinear damping term D_N, gravity and buoyancy term $g(\eta)$, and external disturbance τ_d. These nonlinear terms and disturbances reflect the real-world forces and dynamic properties of the system in complex marine environments, particularly highlighting how environmental changes introduce nonlinear influences on system motion.

The sliding mode surface is the core of sliding mode control. By designing an appropriate sliding mode surface, the system's state can gradually approach and slide along the surface until it reaches the equilibrium point. However, in complex dynamic environments, the intensity of external disturbances often varies significantly. A single-scale sliding mode surface may struggle to balance both robustness and precision when subject to varying disturbance conditions. Larger external disturbances require stronger control actions to ensure system robustness, while smaller disturbances necessitate finer control to avoid over adjustment. Multiple sliding mode surfaces are designed to respond to different levels of disturbances and changes in the system state. The large-scale sliding mode surface handles stronger external disturbances to ensure robustness, while small-scale sliding mode surface provides finer control for smaller disturbances, guaranteeing accuracy and stability.

2.4.1. Large-Scale Sliding Mode Surface

A multi-scale sliding mode surface is proposed, incorporating a parameter that consists of both a fixed and a dynamically varying component. This hybrid design allows for adaptive responses to external disturbances of varying intensities, ensuring robustness during large disturbances, while maintaining precision for smaller disturbances. The large-scale sliding mode surface for handling strong disturbances can be written as indicated in Equation (5):

$$s_1(x) = (\lambda_1 + \lambda_d(t))e(t) + \dot{e}(t) \tag{5}$$

where $e(t) = \eta_d - \eta$ is the tracking error, $\dot{e}(t)$ is the error derivative, η_d represents the designed path, and η is the current trajectory. Moreover, λ_1 is the fixed-gain component, responsible for the system's baseline response; $\lambda_d(t)$ represents the dynamic adaptive gain; while $\dot{\lambda}_d = \xi|e(t)|$; ξ is a positive scalar coefficient that regulates the rate of adaptation; and $\dot{e} = \dot{\eta}_d - \dot{\eta}$.

2.4.2. Small-Scale Sliding Mode Surface

For smaller disturbances requiring fine-tuned control, the small-scale sliding mode surface is defined in Equation (6):

$$s_2(x) = \lambda_2 e(t) + \dot{e}(t) \tag{6}$$

where λ_2 represents a fixed, smaller gain designed for precise control under conditions of minimal disturbances. This gain ensures stability and reduces overshoot by providing a more refined control action. In these mild disturbance conditions, the control system avoids excessive responses and maintains trajectory accuracy without requiring significant adjustments.

2.4.3. Multi-Scale Sliding Mode Surface Combination

The overall sliding mode surface is a weighted combination of the large-scale and small-scale sliding mode surfaces, as expressed in Equation (7):

$$s(x) = \alpha_1 s_1 + \alpha_2 s_2 \tag{7}$$

where α_1, α_2 are time-varying weighting factors, such that $\alpha_1 + \alpha_2 = 1$. This formulation allows the controller to prioritize the large-scale sliding mode surface when disturbances are significant, while relying on the small-scale surface for precision control when subject to milder conditions. So, the small changes in the surface of the sliding mode, or the derivative, can be written as in Equation (8): Considering the variation of the sliding mode surface for large-scale and small-scale disturbances, the equation can be derived as shown in Equation (8):

$$\dot{s} = (\alpha_1 + \alpha_2)\ddot{e} + 2\alpha_1\xi e\dot{e} + (\alpha_1\lambda_1 + \alpha_2\lambda_2)\dot{e} = \ddot{e} + 2\alpha_1\xi e\dot{e} + (\alpha_1\lambda_1 + \alpha_2\lambda_2)\dot{e} \tag{8}$$

Substitute the dynamics equation into the error equation to obtain $\ddot{e} = \ddot{\eta}_d - \ddot{\eta} = \ddot{\eta}_d - (p_1(x,t) + p_2(x,t) + p_3(x,t))$.

Then, the surface of the sliding mode can be written as shown in Equation (9):

$$\dot{s} = \ddot{\eta}_d - (p_1(x,t) + p_2(x,t) + p_3(x,t)) + 2\alpha_1\xi e\dot{e} + (\alpha_1\lambda_1 + \alpha_2\lambda_2)\dot{e} \tag{9}$$

2.4.4. Control Law Design

Considering the sliding mode function s, to mitigate the chattering problem typically associated with it, the function can be redesigned using a saturation function, which smooths the control action near the sliding surface. Thus, the derivative of the sliding mode function s is designed using a saturation function to smooth the control input and reduce the chattering effect, ensuring more stable control performance. That is, $\dot{s} = -k_1 s + k_2 sat(s/\vartheta)$, $k_1, k_2 > 0$, ϑ is the thick of boundary and the control law can be designed as in Equation (10):

$$\tau \quad = M\ddot{\eta}_d - M(2\alpha_1\xi e\dot{e} + (\alpha_1\lambda_1 + \alpha_2\lambda_2)\dot{e}) + C(\eta)\dot{\eta} + D(\eta)\eta + g(\eta) - \tau_d \tag{10}$$

2.4.5. Dynamic Compensation Methods

The dynamic compensator not only adjusts the control inputs in real time to address instantaneous disturbances and uncertainties within the system, but also compensates for the external disturbances by estimating them in real time, ensuring the stability of the ROV in complex marine environments. By quickly responding to external disturbances and actively correcting errors caused by such disturbances, the dynamic compensator significantly enhances the system's dynamic response speed and overall control accuracy. This design strengthens the robustness of the system, enabling precise control even in varying ocean conditions. Considering the control and s function, along with the dynamic compensator, the control law can be written as given in Equation (11):

$$\tau = M\ddot{\eta}_d - M(2\alpha_1\xi e\dot{e} + (\alpha_1\lambda_1 + \alpha_2\lambda_2)\dot{e}) + C(\eta)\dot{\eta} + D(\eta)\dot{\eta} + g(\eta) - k_1 s - k_2 sat(s/\vartheta) + h - \tau_d \tag{11}$$

The mechanism is a dynamic compensator used to enhance the system's response speed, $\alpha, \beta > 0$. $\dot{h} = -\alpha h + \beta s$. To handle both the sliding mode surface s and the disturbance τ_d, two adaptive parameters, one for the adaptive adjustment of the sliding mode surface and the other for estimating and compensating the disturbance, are designed as indicated in Equation (12):

$$\dot{k}_1 = \gamma_1 s^2, \dot{k}_2 = \gamma_2 s sat(s/\vartheta) \tag{12}$$

where γ is the parameter of adaptive control as in Formula (13).

$$\dot{\hat{\tau}}_d = -\varepsilon s \tag{13}$$

where $\varepsilon > 0$. Therefore, the final control law is designed as shown in Equation (14):

$$\tau = M\ddot{\eta}_d + M(2\alpha_1\xi e + (\alpha_1\lambda_1 + \alpha_2\lambda_2))\dot{\eta}_d + C(\eta)\dot{\eta} + D(\eta)\dot{\eta} + g(\eta) - k_1\hat{s} - k_2 sat(\hat{s}/\vartheta) + h - \hat{\tau}_d \tag{14}$$

This formulation ensures that the system can quickly and accurately respond to disturbances, while maintaining stability and precision in varying marine conditions.

2.5. Stability Analysis of Multi-Scale Sliding Mode Control

In this study, the second Lyapunov method is employed to analyze the stability of the proposed control strategy. Compared to other commonly used stability analysis methods, the Lyapunov method offers distinct advantages, particularly in regard to the stability analysis of nonlinear systems. The second Lyapunov method does not rely on system linearization assumptions, which allows it to handle complex nonlinear systems and significant disturbances, making it especially suitable for systems such as those relating to underwater robots that are characterized by a high level of nonlinearity and uncertainty. In contrast, Linear Matrix Inequality (LMI) methods, although applicable to linear or quasi-linear systems, offer limited capacity for robust stability analysis of nonlinear systems, as they require precise modeling. The Lyapunov method, however, ensures a stronger guarantee of global stability by constructing an appropriate Lyapunov function. Additionally, methods like linear system theory and the small gain theorem are mainly applicable to linear or linearized systems, and are ineffective in addressing the stability of highly nonlinear systems, such as underwater robots [5,9,15]. Therefore, the second Lyapunov method provides a suitable tool for stability analysis in this study, ensuring the effectiveness and robustness of the proposed control strategy within complex systems.

The Lyapunov function for the above design is constructed as given in Formula (15):

$$V = \frac{1}{2}s^2 + \frac{1}{2\alpha}h^2 + \frac{1}{2\gamma_1}(k_1 - k_{10})^2 + \frac{1}{2\gamma_2}(k_2 - k_{20})^2 + \frac{\varepsilon}{2}(\hat{\tau}_d - \tau_d)^2 \tag{15}$$

where k_{10}, k_{20} are the given values of their respective parameters. Obviously $V > 0$, so its derivative can be expressed as in Equation (16):

$$\dot{V} = s\dot{s} + \frac{1}{\alpha}h\dot{h} + \frac{1}{\gamma_1}(k_1 - k_{10})\dot{k}_1 + \frac{1}{\gamma_2}(k_2 - k_{20})\dot{k}_2 + \varepsilon(\hat{\tau}_d - \tau_d)(\dot{\hat{\tau}}_d - \dot{\tau}_d) \tag{16}$$

Substitute Equations (5)–(15) into the expression, and the function can be rewritten as in Equation (17):

$$\begin{aligned}\dot{V} &= s(-(k_1 s + k_2 sat(s/\vartheta) + h) + \tfrac{1}{\alpha}h(-\alpha h + \beta s) + \tfrac{1}{\gamma_1}(k_1 - k_{10})\dot{k}_1 + \tfrac{1}{\gamma_2}(k_2 - k_{10})\dot{k}_2 + \varepsilon(\hat{\tau}_d - \tau_d)(\dot{\hat{\tau}}_d - \dot{\tau}_d) \\ &= -s(k_1 s + k_2 sat(s/\vartheta)) + sh - h^2 + \beta/\alpha sh + (k_1 - k_{10})s^2 + (k_2 - k_{20})ssat(s/\vartheta) - \varepsilon^2(\hat{\tau}_d - \tau_d)^2\end{aligned} \tag{17}$$

Then:

$$\begin{cases} -s(k_1 s + k_2 sat(s/\vartheta) = -k_1 s^2 - k_2 ssat(s/\vartheta) \\ (k_1 - k_{10})s^2 = k_1 s^2 - k_{10} s^2 \\ (k_2 - k_{20})ssat(s/\vartheta) = k_2 ssat(s/\vartheta) - k_{20} ssat(s/\vartheta) \end{cases} \tag{18}$$

According to the Cauchy–Schwarz inequality, the terms can be handled as shown in Equation (19):

$$\begin{cases} sh \le \sqrt{s^2}\sqrt{h^2} = |s||h| \le \frac{s^2}{2c_1} + \frac{c_1 h^2}{2} \\ \frac{\beta}{\alpha}sh \le \frac{\beta}{\alpha}(\frac{s^2}{2c_2} + \frac{c_2 h^2}{2}) \end{cases} \tag{19}$$

where c_1, c_2 are intermediate parameters used for adaptive adjustment. So, $\dot{V}$ can be written as in Equation (20):

$$\begin{aligned}\dot{V} &= \frac{s^2}{2c_1} + \frac{c_1 h^2}{2} - h^2 + \frac{\beta}{\alpha}\left(\frac{s^2}{2c_2} + \frac{c_2 h^2}{2}\right) - k_{10}s^2 - k_{20}ssat(s/\vartheta) - \varepsilon^2\left(\hat{\tau}_d - \tau_d\right)^2 \\ &\leq \left(\frac{1}{2c_1} + \frac{\beta}{2c_2\alpha} - k_{10}\right)s^2 + \left(\frac{c_1}{2} + \frac{c_2\beta}{2\alpha} - 1\right)h^2 - k_{20}|s|^2 - \varepsilon^2\left(\hat{\tau}_d - \tau_d\right)^2\end{aligned} \tag{20}$$

Except for the first and second terms, all other terms are evidently negative, by choosing appropriate positive definite parameters $\alpha, \beta, c_1, c_2, k_{10}, k_{20}, \varepsilon$, so that the first and second terms are negative, then:

$$\dot{V} \leq 0 \tag{21}$$

According to Lyapunov's theorem, the system has been proven to be stable.

3. Simulation and Analysis of ROV Control Performance

3.1. Simulation Setup and Assumptions

As noted in the background information, biofouling significantly affects water quality and aquaculture productivity, emphasizing the importance of effective control measures. Therefore, the development of underwater cleaning ROV for aquaculture has significant practical importance, with one of the key technical challenges being the precise 6-DOF trajectory tracking of ROVs.

The ROV used in this study is designed for the breeding cabins in GUOXIN 1 aquaculture vessels, where the cabin dimensions are 19,500 mm in length, 22,500 mm in width, and 14,500 mm in height. During the experimental phase, the ROV tests were conducted in a water pool to simulate the conditions of the cabin and eliminate the effects of external waves and currents. The experimental water pool was set to a static water environment, primarily to test the basic control functions of the ROV. Figure 3 shows the experimental setup: (a) the breeding cabin in the aquaculture vessel and (b) the ROV for cleaning.

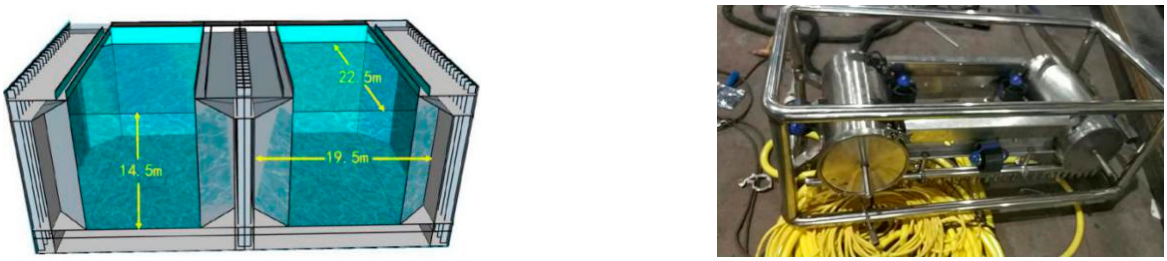

(**a**) (**b**)

Figure 3. Schematic of breeding cabin and experimental ROV. (**a**) The breeding cabin in an aquaculture vessel. (**b**) The ROV for cleaning.

Before performing the simulation analysis, the following assumptions were made based on actual working conditions and the existing literature. These assumptions are grounded in regard to the use of a Gaussian distribution to provide a simplified, yet accurate, approximation of large-scale disturbances in marine environments, while smaller turbulence effects can be ignored. Previous studies have shown that in complex marine environments, such as shallow waters, multi-directional waves, or confined waters, wave dynamics exhibit significant nonlinear characteristics and variability. Therefore, using a Gaussian distribution to simulate large-scale external disturbances, while ignoring localized turbulence effects, is an effective method for simplifying the control system [19–21].

Assumption 1. *In deep-sea environments, wave activity is minimal, and the dynamic changes in the aquaculture vessel are relatively slow, so it can be considered stable.*

Assumption 2. *The exchange of water within the cabin, fish movements, equipment operation, and the oscillation of the vessel due to wind and waves can be modeled using a Gaussian distribution [18]. Additionally, the internal forces generated by the interaction between the ROV, waves, and water flow must also be considered.*

Assumption 3. *The reaction forces generated by high-pressure water jets can be automatically balanced by the ROV's X-axis thrusters. Under high-pressure water jet conditions, the turbulence effects are minimal and external environmental disturbances can be neglected.*

The mechanism aims to overcome the limitations of existing systems in complex marine environments. To validate the effectiveness of the proposed control algorithm, experiments will be conducted in a controlled water environment, with a focus on evaluating the system's performance in handling nonlinear characteristics and external disturbances.

3.2. Numerical Simulations of ROV Tracking

In this section, numerical simulations are conducted involving the self-developed ROV. The simulations include the following scenarios:

Trajectory Tracking Performance Test: Simulate the ROV's movement along a predefined trajectory to evaluate its trajectory tracking capability and tracking error. The analysis focuses on the ROV's trajectory tracking performance under different speeds and turning angles, with an emphasis on measuring the control rate and tracking error to ensure the ROV can stably follow the predefined path.

Control Strategy Comparison: A comparison is made between adaptive terminal sliding mode control (ATSMC), non-adaptive terminal sliding mode control (NTSMC), and MDSMAC, by simulating the ROV's trajectory tracking under different disturbance conditions to evaluate the performance of each control strategy. The key metrics measured are the tracking error, disturbance estimation, and control rate, in order to validate the effectiveness of MDSMAC in controlling the ROV's motion in various environments. The simulation tests will compare the three control strategies by assessing their performance in terms of trajectory tracking accuracy, disturbance compensation, and control rate, thus verifying the advantages of MDSMAC.

Long-term Operational Stability Simulation: Simulate the robot's stability and control performance under continuous long-term operation.

The ROV designed by our team is shown in Figure 3b. The ROV has dimensions of 1.1 m in length, 0.4 m in width, and 0.6 m in height, with the center of gravity assumed to coincide with the center of buoyancy, resulting in zero offset values for x_g, y_g, z_g. Its detailed parameters are listed in Table 1 below.

The Coriolis matrix C is derived based on the standard underwater vehicle dynamics framework [2], and is formulated as indicated in Equation (22):

$$C = \begin{bmatrix} 0 & 0 & 0 & 0 & -m \cdot w & m \cdot v \\ 0 & 0 & 0 & m \cdot w & 0 & -m \cdot u \\ 0 & 0 & 0 & -m \cdot v & m \cdot u & 0 \\ 0 & -m \cdot w & m \cdot v & 0 & -I_z \cdot r & I_y \cdot q \\ m \cdot w & 0 & -m \cdot u & I_z \cdot r & 0 & -I_x \cdot p \\ -m \cdot v & m \cdot u & 0 & -I_y \cdot q & I_x \cdot p & 0 \end{bmatrix} \tag{22}$$

The hydrodynamic damping coefficients were estimated using empirical formulas based on standard hydrodynamic theory [3,14,22]. The linear damping coefficients were derived from a viscous drag model, while the quadratic damping coefficients were obtained using empirical drag coefficients specific to cylindrical bodies.

$$D = \text{diag}\left(X_u + X_{|u|u}\left|u\right|, Y_v + Y_{|v|v}\left|v\right|, Z_w + Z_{|w|w|}\left|w\right|, K_p + K_{|p|p}\left|p\right|, M_q + M_{|q|q|}\left|q\right|, N_r + N_{|r|r}\left|r\right|\right) \quad (23)$$

Table 1. ROV simulation parameters.

Parameters	Symbol	Value	Unit	Parameters	Symbol	Value	Unit
Mass	m	21.07	kg	Rotational inertia	I_x	0.70	kgm^2
Buoyancy	B	358.18	N	Rotational inertia	I_y	2.18	kgm^2
Gravity	W	350.49	N	Rotational inertia	I_z	2.80	kgm^2
Volume	V	0.0035	m^3	Barycenter	Z_W	0.42	m

In this study, the hydrodynamic damping coefficients were estimated using empirical formulas to represent the ROV's hydrodynamic characteristics. The linear damping coefficient D primarily accounts for viscous drag, calculated as given in Equation (24):

$$D_i = C_{linear} A_i \rho \quad (24)$$

The damping coefficients are uniformly denoted as D_i, where i represents the six directions and angles $x, y, z, \varphi, \psi, \theta$, the following formulas apply similarly. Where C_{linear} is the dimensionless linear damping coefficient, A_i represents the reference cross-sectional area of the ROV, and ρ is the fluid density.

The quadratic damping coefficient $D_{|i|i}$, which reflects drag forces, is applied for nonlinear damping terms and is shown in Equation (25):

$$D_{|i|i} = C_{di} A_i \rho \quad (25)$$

where C_{di} is the drag coefficient, typically determined based on the shape of the object (e.g., for cylindrical objects, $C_d \approx 0.47$). These damping coefficients are used to construct the damping matrix D for the ROV, accounting for the hydrodynamic effects in a freshwater environment.

3.3. Trajectory Tracking Performance

The parameters are given: $\lambda_1 = 5$, $\lambda_2 = 0.05$, $k_1 = k_2 = 0.05$, $\vartheta = 0.1$, $\alpha_1 = 1$, $\alpha_2 = 1$, $\gamma = 50$, and $\varepsilon = 50$. The simulation time is set to 20 s, with a step size of 0.001 s. The initial state is set to $\eta_0 = [0;\ 10;\ 0;\ 0;\ 0;\ 0]^T$,$\eta_d = [10\sin(at); 10\cos(at); \text{bt}, zeros(3, N)]$,$\tau_{disturbance} = 100rand$.

Figure 4 illustrates the 6-DOF trajectory tracking, demonstrating that despite structural nonlinearities and significant Gaussian disturbances, the control strategy rapidly adjusts to align with the reference trajectory across all the axes. The angular deviations in regard to the roll, pitch, and yaw remain minimal, within approximately 0.2°. In the X, Y, and Z directions, trajectory tracking is achieved with minor fluctuations in the tracking errors due to persistent Gaussian disturbances. These results indicate that the controller effectively maintains accurate trajectory tracking in all directions.

Under significant Gaussian external disturbances and the influence of structural nonlinearities, the designed control law exhibits corresponding fluctuations, while automatically adapting to these disturbances. Figure 5 illustrates the variations in the control input, where the combined effects of structural nonlinearities and external disturbances result in oscillations around a baseline value. The numerical simulation results demonstrate that this multi-scale dynamic sliding mode adaptive control strategy effectively achieves stable trajectory tracking in conditions involving structural nonlinearities and disturbance uncertainty, exhibiting strong adaptability and robustness.

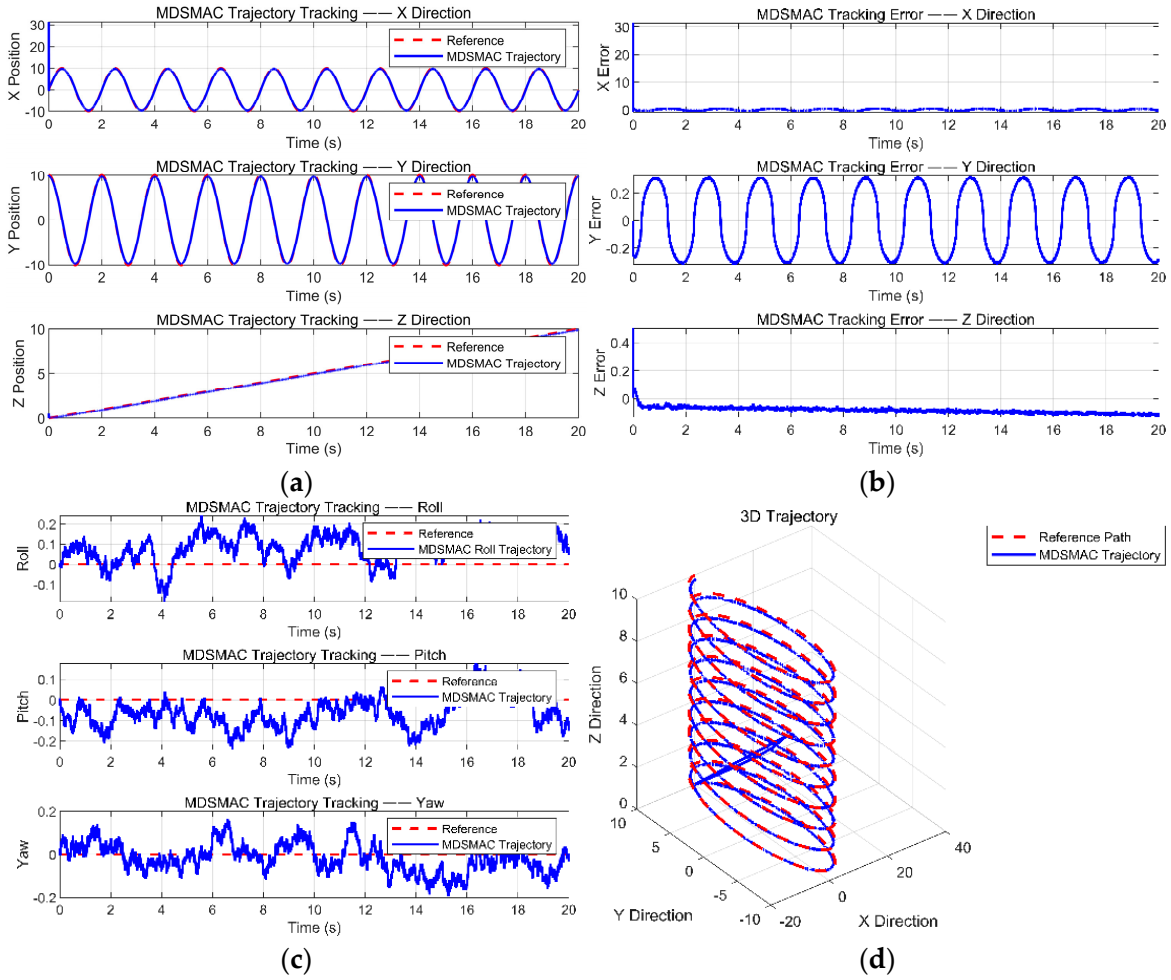

Figure 4. Trajectory tracking and tracking error: (**a**) position tracking, (**b**) position tracking error, (**c**) angle tracking, (**d**) 3D trajectory.

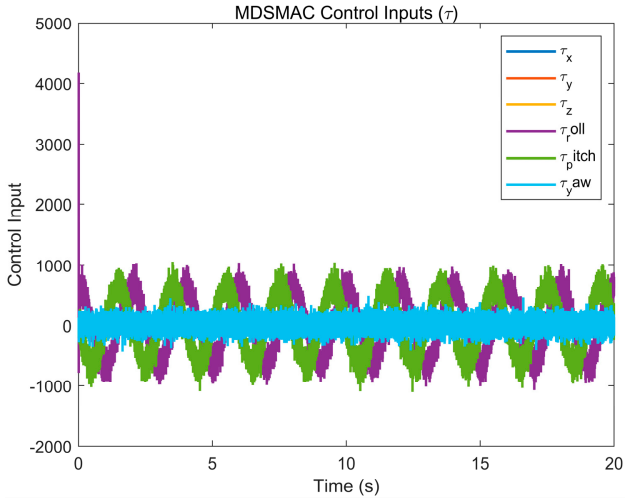

Figure 5. Total control.

The mean of the disturbance estimates across multiple degrees of freedom is approximately zero, indicating effective overall performance, as in Figure 6. The numerical simulation results demonstrate that multi-scale dynamic sliding mode adaptive control achieves

reliable tracking control in conditions involving structural nonlinearities and disturbance uncertainty, balancing external disturbances effectively and exhibiting strong robustness.

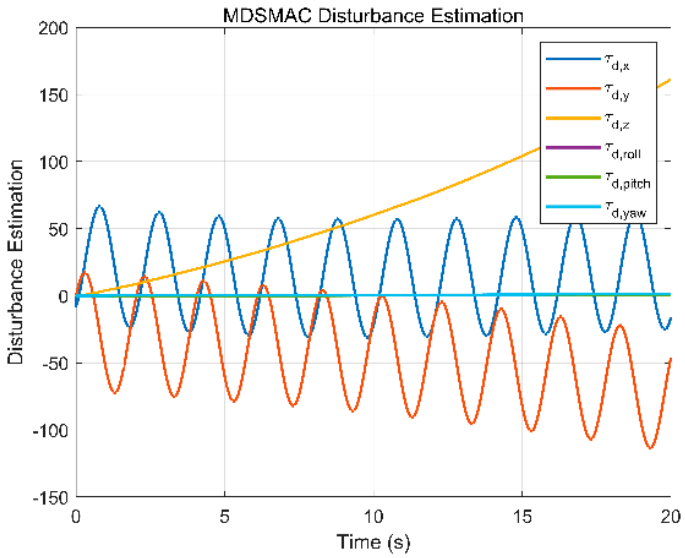

Figure 6. Adaptive disturbance estimation.

3.4. Control Strategy Comparison

Numerical simulations and comparative analyses were conducted in regard to the three control strategies, including non-adaptive terminal sliding mode control, adaptive terminal sliding mode control, and multi-scale dynamic sliding mode adaptive control [23–26]. In this section, a comparison is first made between traditional control methods (such as PID control and FLC control) and the multi-scale dynamic sliding mode adaptive control (MDSMAC) algorithm proposed in this study. Then, the performance of Non-Singular Sliding Mode Control (NS-SMC), adaptive terminal sliding mode control (AT-SMC), and MDSMAC under various disturbance conditions is analyzed. Through these comparisons, this study aims to investigate the advantages and disadvantages of each control strategy in terms of trajectory tracking accuracy, system stability, and robustness to complex disturbances, and further analyzes the strengths and limitations of each approach.

3.4.1. Comparison with Traditional Algorithms

This section presents a comparative analysis of traditional control methods, including PID control, FLC, traditional SMC, and NNC, with the multi-scale dynamic sliding mode adaptive control (MDSMAC) strategy proposed in this study. The comparisons are conducted based on identical reference paths, static ROV parameters, external disturbances, and dynamic parameter conditions. All of the results are shown in Figures 7 and 8.

Subject to the same input and external disturbance conditions, the simulation tests show that only the proposed multi-scale dynamic sliding mode adaptive control (MDSMAC) and traditional SMC achieve effective trajectory tracking. The standalone NNC and FLC fail to fully accomplish trajectory tracking, while PID control achieves preliminary tracking, but requires further parameter adjustments to attain precise tracking. Differences in performance are also evident in terms of the vacancy rate and error across the control strategies.

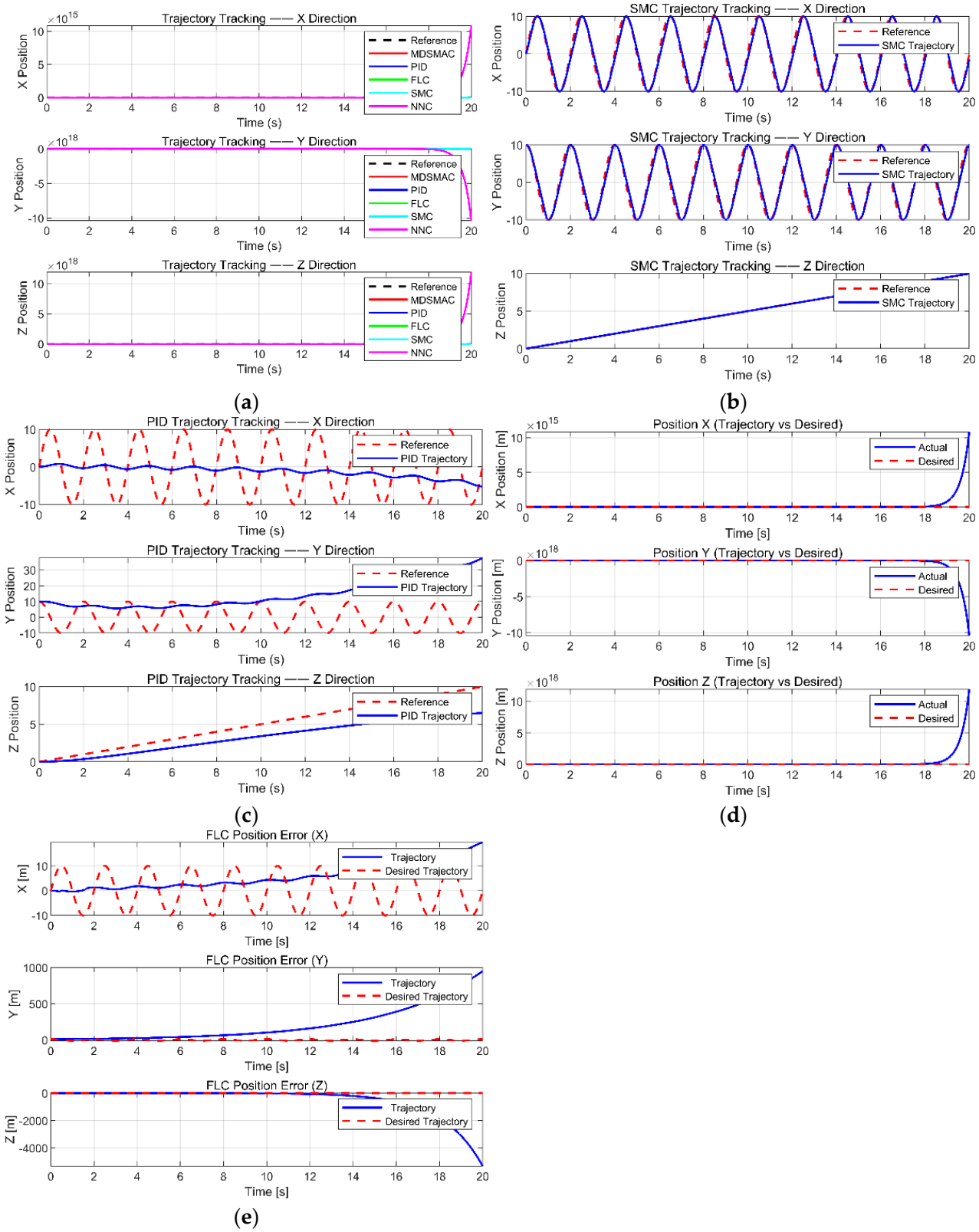

Figure 7. Comparison of trajectory tracking performance between MDSMAC and traditional algorithms: (**a**) trajectory tracking comparison between MDSMAC and traditional algorithms, (**b**) trajectory tracking using traditional SMC, (**c**) trajectory tracking using PID, (**d**) trajectory tracking using NNC, (**e**) trajectory tracking using FLC.

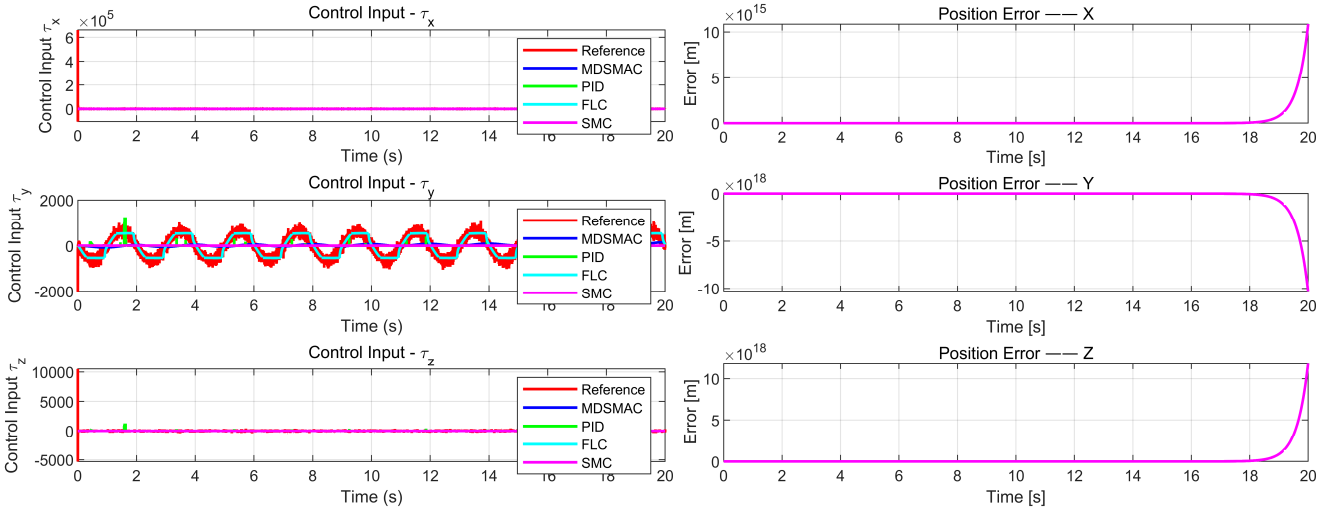

(**a**) (**b**)

Figure 8. Comparison of control rates and errors between the proposed and traditional algorithms: (**a**) comparison of control rates between the proposed algorithm and traditional algorithms, (**b**) comparison of tracking errors between the proposed algorithm and traditional algorithms.

3.4.2. Comparison When Subject to Minor Stochastic Disturbances

The parameters are given: $\lambda_1 = 5$, $\lambda_2 = 0.05$, $k_1 = k_2 = 0.05$, $\vartheta = 0.1$, $\alpha_1 = 1$, $\alpha_2 = 1$, $\gamma = 50$, and $\varepsilon = 50$. The simulation time is set to 20 s, with a step size of 0.001s. The initial state is set to $\eta_0 = [0;\ 10;\ 0;\ 0;\ 0;\ 0]^T$, $\eta_d = [10\sin(at); 10\cos(at); bt, zeros(3, N)]$,$\tau_{disturb1} = rand$, and $\tau_{disturb10} = 10rand$.

As observed in Figure 9a,b, when subject to low disturbance magnitudes, all three strategies, MDSMAC, ATSMC, and NTSMC, can generally track the predefined trajectory, although NTSMC exhibits lower tracking accuracy. From the tracking error plots in (c) and (d), it is evident that NTSMC shows significantly higher fluctuations than the other two strategies, with MDSMAC demonstrating the highest error stability. In the disturbance estimation plots (e) and (f), both MDSMAC and ATSMC effectively estimate disturbance variations, with MDSMAC showing the best responsiveness to disturbance changes, while NTSMC lacks disturbance estimation capability.

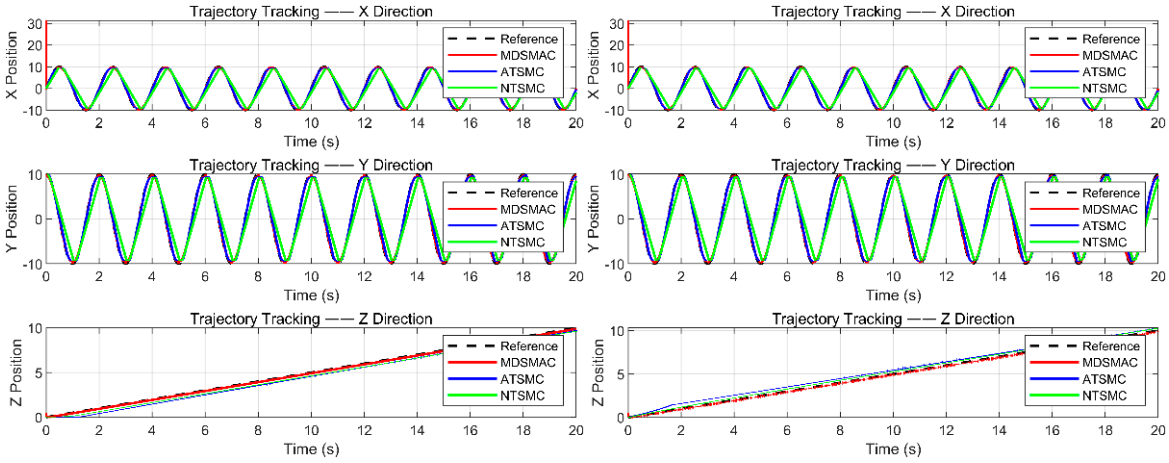

(**a**) (**b**)

Figure 9. *Cont.*

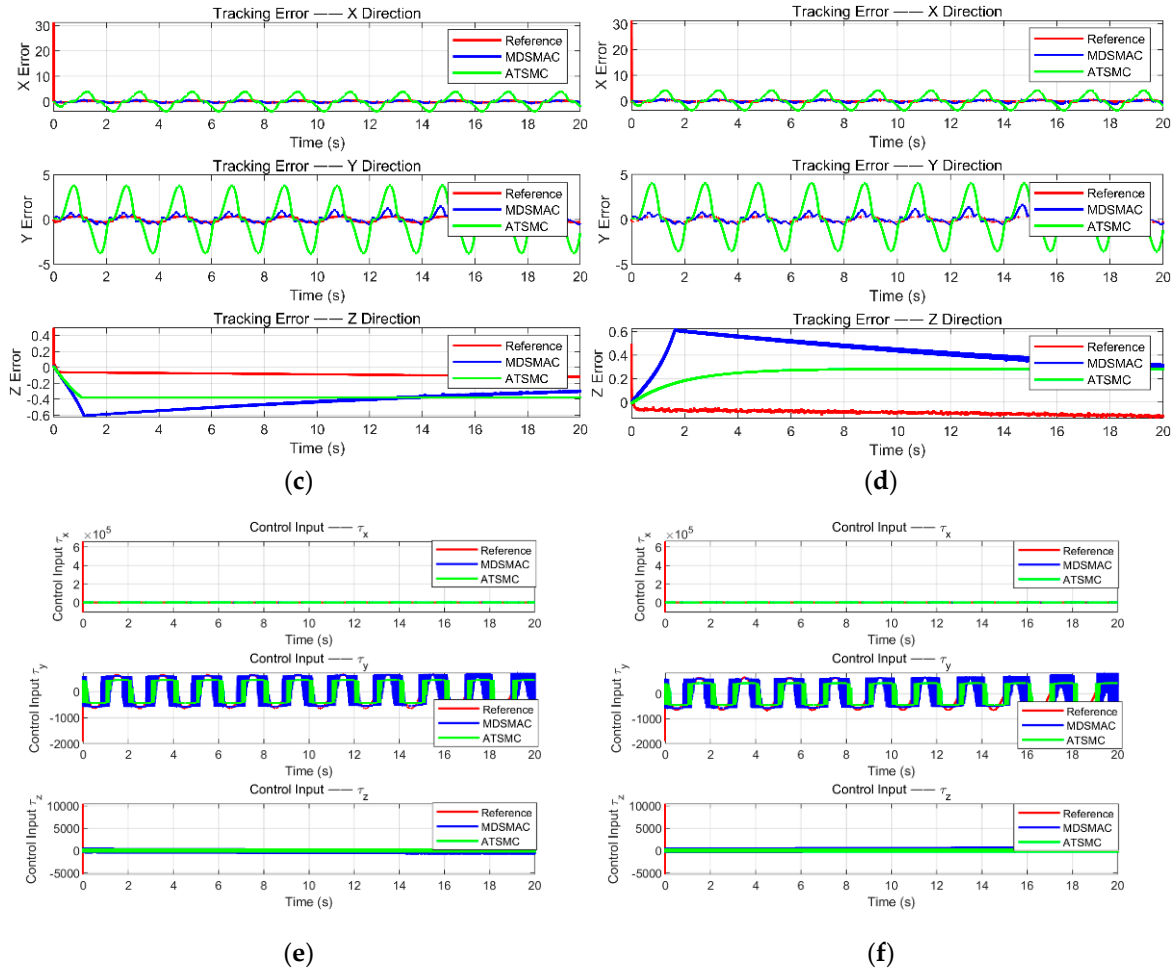

Figure 9. Trajectory tracking in XYZ directions with different control strategies: (**a**) comparison of tracking when subject to a single disturbance, (**b**) comparison of tracking when subject to tenfold disturbance, (**c**) comparison of errors when subject to a single disturbance, (**d**) comparison of errors when subject to tenfold disturbance, (**e**) comparison when subject to a single Gaussian disturbance, (**f**) comparison when subject to tenfold Gaussian disturbance.

Table 2 presents the mean squared error (MSE) and mean absolute error (MAE) for each control strategy in regard to trajectory tracking. The comparison reveals that MDSMAC consistently achieves lower errors in the x, y, and z directions, demonstrating significantly higher tracking accuracy, disturbance rejection capabilities, and response speed than the other strategies.

Table 2. Comparison of tracking data.

(a) Mean Squared Error				**(b) Mean Absolute Error**			
Control Strategy	*X*	*Y*	*Z*	Control Strategy	*X*	*Y*	*Z*
MDSMAC	0.205	0.063	0.008	MDSMAC	0.269	0.239	0.087
ATSMC	0.341	0.256	0.187	ATSMC	0.400	0.365	0.411
NTSMC	5.269	5.433	0.137	NTSMC	1.805	1.824	0.367

In terms of the MSE, MDSMAC yields the lowest error in all directions, with a particularly low value of 0.008 in the Z-direction, which is substantially lower than that of ATSMC and NTSMC. This suggests that MDSMAC can maintain stable tracking in terms of the predefined trajectory even under considerable disturbances. However, due to external

disturbances and the inherent nonlinear structure of the ROV, it is not feasible for any control strategy to achieve perfect trajectory adherence at all times in complex operational environments. Nonetheless, MDSMAC displays superior response speed and disturbance resilience, effectively minimizing errors over time and maintaining close alignment with the target trajectory. Nonetheless, MDSMAC exhibits enhanced response speed and improved disturbance resilience, effectively minimizing errors over time and maintaining close alignment with the target trajectory.

In regard to the MAE, MDSMAC again outperforms the other strategies, with errors of 0.269, 0.239, and 0.087 in the X, Y, and Z directions, respectively, which are consistently lower than those of ATSMC and NTSMC. This further substantiates MDSMAC's precision control across multiple axes. In contrast, ATSMC shows moderately higher MAE values, indicating a degree of adaptability, but lower robustness compared to MDSMAC. NTSMC, however, exhibits considerably larger MAE values in the X and Y directions (1.805 and 1.824, respectively), suggesting limited capacity for disturbance compensation and posing potential challenges for precise control in real-world applications.

While control strategies cannot entirely eliminate error in highly nonlinear and disturbance-prone environments, MDSMAC demonstrates superior response speed and tracking accuracy in all directions, making it the optimal control solution for stable tracking in complex disturbance conditions.

3.4.3. Significant Environmental Stochastic Disturbances

The parameters are given: $\lambda_1 = 5$, $\lambda_2 = 0.05$, $k_1 = k_2 = 0.05$, $\vartheta = 0.1$, $\alpha_1 = 1$, $\alpha_2 = 1$, $\gamma = 50$, and $\varepsilon = 50$. The simulation time is set to 20 s, with a step size of 0.001 s. The initial state is set to $\eta_0 = [0.1;\ 1;\ 0;\ 0;\ 0;\ 0]^T$, $\eta_d = [10\sin(at); 10\cos(at); bt, zeros(3, N)]$, $\tau_{disturb100} = 100rand$.

As shown in Figure 10a–c, the performance of different control strategies in regard to trajectory tracking varies significantly. MDSMAC effectively completes the tracking task when subject to strong disturbances, demonstrating superior disturbance rejection and tracking accuracy. In contrast, ATSMC struggles to maintain stable tracking when subject to large disturbances, and NTSMC exhibits substantial tracking errors, making precise trajectory tracking unachievable. These results highlight the clear advantages of MDSMAC in handling complex disturbances, providing a more reliable solution for accurate trajectory tracking.

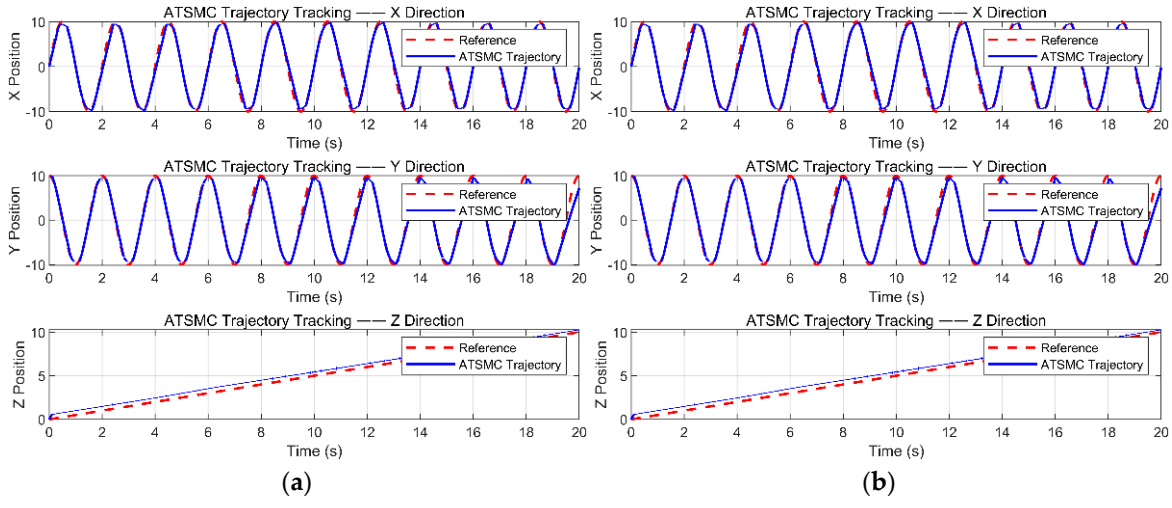

Figure 10. *Cont.*

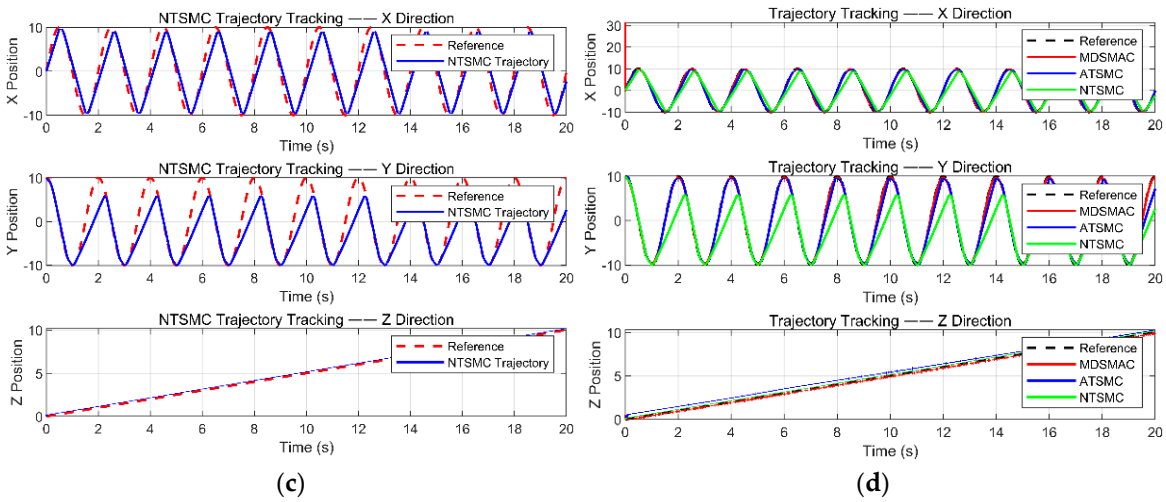

Figure 10. Trajectory tracking under different control strategies with strong Gaussian disturbance: (**a**) trajectory tracking with MDSMAC, (**b**) trajectory tracking with ATSMC, (**c**) trajectory tracking with NTSMC, (**d**) comparison between trajectory tracking among the three methods.

In regard to both strong and mild disturbance conditions, the MDSMAC strategy consistently demonstrates optimal performance. Even with persistent structural nonlinearities, it achieves high-precision trajectory tracking and robust disturbance rejection, outperforming other control methods.

3.5. Long-Term Operational Stability Simulation

The parameters are given: $\lambda_1 = 0.05$, $\lambda_2 = 0.005$, $k_1 = k_2 = 0.05$, $\vartheta = 0.1$, $\alpha_1 = 1$, $\alpha_2 = 1$, $\gamma = 10$, and $\varepsilon = 0.02$. The simulation time is set to 100,000 s, with a step size of 1 s. The initial state is set to $\eta_0 = [0; 10; 0; 0; 0; 0]^T$,$\eta_d = [10\sin(at); 10\cos(at); bt, zeros(3, N)]$,$\tau_{disturb} = rand$. Long-term operation is an essential requirement for task-oriented ROVs and control stability is a necessary characteristic. To evaluate the controllability and stability of the control system, a simulation was conducted for a full day (100,000 s), with a time step of 1 s. This long-term simulation allows for a comprehensive assessment of the controller's performance and stability over extended periods, verifying its effectiveness in practical applications.

As shown in Figure 11, the designed scheme demonstrates excellent trajectory tracking performance over an extended period. Throughout the simulation, the ROV closely adheres to the predefined path, maintaining stable operation, and showcasing the robustness and long-term operational capability of the scheme in the presence of external disturbances and structural nonlinearities. In both 2D and 3D trajectory tracking, the tracking error remains minimal, with the system showing very little deviation from the intended path. Overall, these results confirm the effectiveness and reliability of the control strategy for long-term applications, demonstrating its ability to maintain consistent and stable performance in complex conditions.

The comprehensive simulation results indicate that the designed control strategy exhibits significant advantages in complex conditions. Firstly, the strategy achieves high-precision trajectory tracking, even in the presence of structural nonlinearities and external disturbances. Secondly, when compared to other control methods, the MDSMAC strategy demonstrates superior tracking accuracy and stability across various disturbance intensities. Lastly, in regard to long-term operation simulations, the strategy shows excellent robustness, maintaining consistent and stable performance in challenging environments.

These findings collectively confirm the efficiency and reliability of the designed control strategy for practical applications.

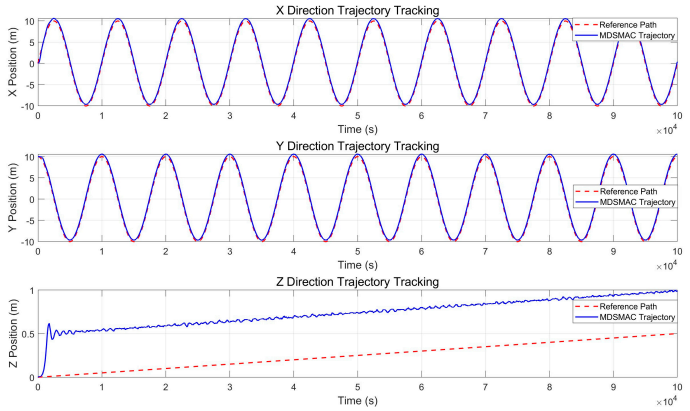

(**a**)

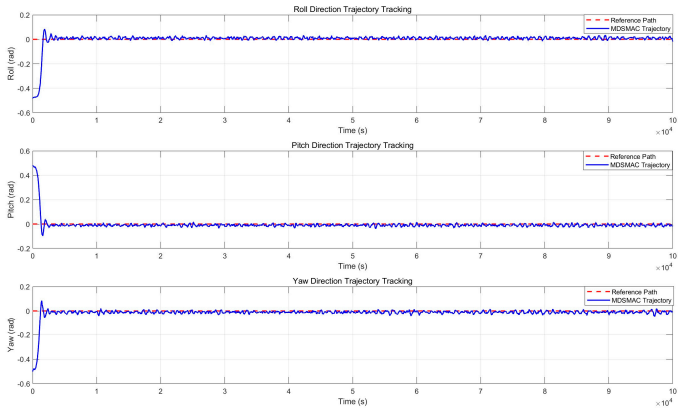

(**b**)

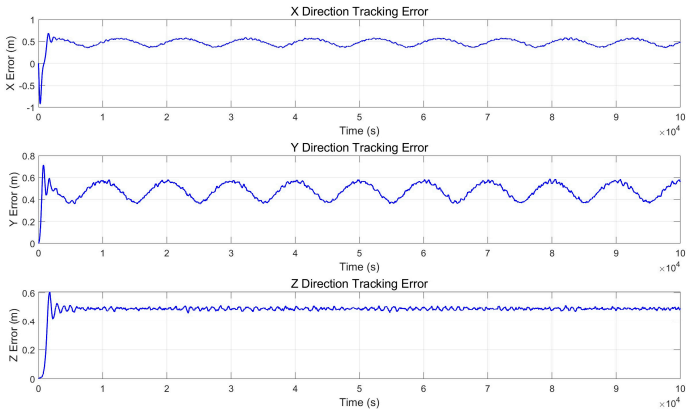

(**c**)

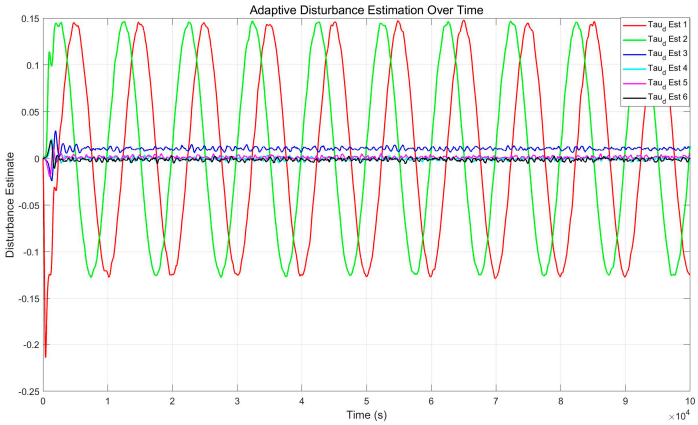

(**d**)

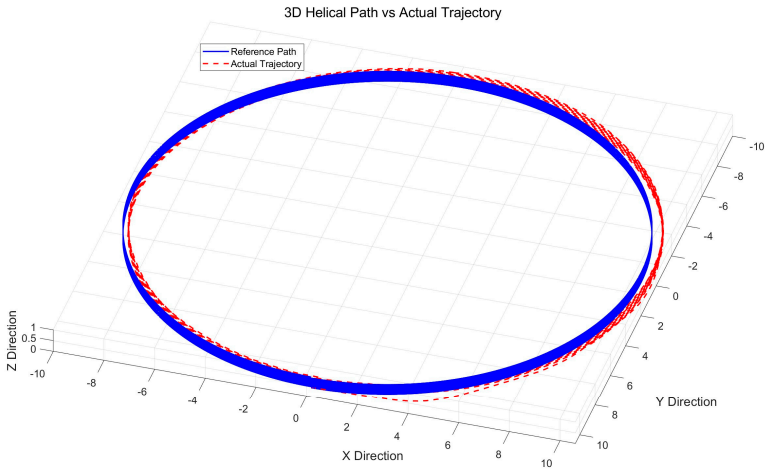

(**e**)

Figure 11. Long-term tracking trajectory under MDSMAC: (**a**) trajectory tracking in XYZ directions; (**b**) trajectory tracking in terms of roll, pitch, and yaw angles; (**c**) tracking errors in XYZ directions; (**d**) adaptive disturbance estimation; (**e**) 3D trajectory tracking.

4. Validation of the Control Strategy Considering Machine Nonlinearities

4.1. Experimental Environment

To further validate the multi-scale dynamic sliding mode adaptive control strategy proposed in this study, experiments were conducted in a testing pool. The objective was to evaluate the MDSMAC's ability to compensate for nonlinear disturbances and to test the stability of the system during long-term operation.

The water pool used for the experiment measures 130 m in length, 6 m in width, and 3.5 m in depth, as shown in Figure 12a. It simulates the operational environment of the underwater cleaning ROV in an aquaculture tank. The in-house developed 6-DOF ROV, shown in Figure 12c, measures 1.2 m in length, 0.4 m in width, and 0.6 m in height. The main buoyancy structure consists of dual floatation cylinders and the external frame is constructed from stainless steel tubing. The thruster configuration is shown in Figure 1, with detailed mass and other parameters listed in Table 1. The ROV is equipped with an Inertial Measurement Unit (IMU), depth sensors, and cameras to support real-time navigation and trajectory tracking.

(**a**) (**b**) (**c**)

Figure 12. Experimental pool environment and robotic system: (**a**) experimental pool, (**b**) robotic control system, (**c**) ROV in pool.

IMU Operational Principles: The Inertial Measurement Unit (IMU) comprises a three-axis accelerometer and a three-axis gyroscope, designed to measure linear acceleration and rotational rates along three orthogonal axes. By fusing data from these sensors, the IMU provides accurate information about the robot's orientation and position.

Pressure-Type Depth Sensor Principles: The pressure-type depth sensor determines the robot's depth by measuring the static water pressure in the underwater environment. As the depth increases, the water pressure increase linearly, and the sensor converts these pressure changes into corresponding depth values. This method ensures that a high level of accuracy and stability are achieved, making it suitable for various underwater operations.

Sensor Installation and Parameters: The IMU's accelerometer range was adjusted to ± 2 g, with a sensitivity of 16,384 LSB/g, and the gyroscope range was set to ± 2000 dps, with a sensitivity of 16.4 LSB/°/s. The depth sensor can measure depths up to 100 m, with an accuracy of 0.1 m. These sensors are installed in the groove of the robot's upper crossbar, ensuring both data acquisition and protection against physical damage.

4.2. Nonlinear System Control Experiment

4.2.1. Experiment Objective MDSMAC Experiment Objective

The aim of this experiment is to validate the effectiveness of the MDSMAC algorithm in handling the nonlinear characteristics of a system, particularly in regard to trajectory tracking tasks. Achieving these objectives will further assess the practicality and efficiency of the MDSMAC system for underwater robotic cleaning operations.

4.2.2. Experimental Procedure MDSMAC Trajectory Tracking Procedure

Trajectory Setup: The ROV follows a predefined trajectory to simulate typical underwater mission paths, including straight lines, arcs, and turns at various depths, to assess the system's trajectory tracking capability.

Internal Disturbance Simulation: Internal disturbances caused by inertia and water resistance are simulated by varying the ROV's speed. The ROV operates at speeds of 0.1 m/s, 0.15 m/s, 0.5 m/s, and 1.0 m/s to test system performance under different conditions. Among these, 0.15 m/s is the ideal speed calculated based on time efficiency requirements for cleaning tasks, 0.1 m/s serves as a low-speed reference, 1.0 m/s simulates high-speed operations, and 0.5 m/s acts as a medium-speed benchmark. These speed variations simulate the effects of different workloads and water resistance, allowing the evaluation of the system's responsiveness in various operational scenarios.

Data Collection and Analysis: During the experiment, the ROV's position, acceleration, and video image data are collected in real time using an Inertial Measurement Unit (IMU) and a camera system. Each test runs for 10 min to assess trajectory deviation, acceleration variations, and control input response characteristics, thereby analyzing the system's performance in terms of internal nonlinear factors.

4.2.3. Experimental Results Comparison of Trajectory Control Performance

To clearly present the experimental data, the data are recorded and the trajectory errors and recovery times are compared under different experimental conditions. This highlights the relationship between trajectory control accuracy and speed, as well as the impact of current limitations observed at higher speeds.

The experimental data are divided into three parts: *Z*-direction, *X*-direction, and *Y*-direction. Trajectory errors and system performance vary across different directions and speeds. Three velocity plots were generated to visually compare the expected and actual speeds in each direction, illustrating the system's performance under different conditions, as shown in Figure 13.

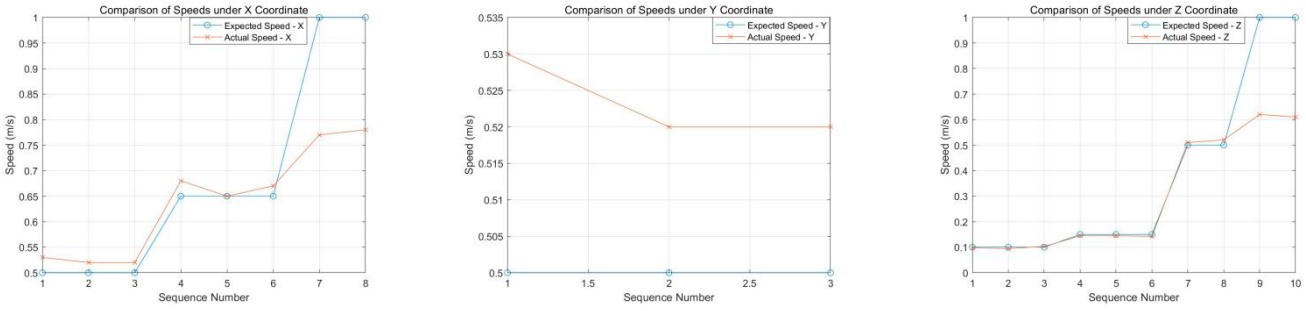

Figure 13. Comparison of expected and actual speed: (**a**) comparison in the *X*-direction, (**b**) comparison in the *Y*-direction, (**c**) comparison in the *Z*-direction.

Z-Direction Test: In the *Z*-direction test, the target speeds are set at 0.1 m/s, 0.15 m/s, 0.5 m/s, and 1 m/s. At low speeds (0.1 m/s and 0.15 m/s), the system performs stably with errors within ±5%, indicating effective compensation for inertial disturbances and nonlinear characteristics. As the speed increases to 0.5 m/s, the error slightly increases to within 4%, an acceptable range. However, at 1 m/s, due to current limitations (insufficient thrust to maintain the speed), the error increases significantly, to a maximum of 39%. This shows that at higher speeds, insufficient current severely impacts control precision, making it difficult to maintain the desired trajectory.

X-Direction Test: In the *X*-direction test, the target speeds are set at 0.5 m/s and 0.65 m/s. The system generally performs well, with errors within ±5.33%. At 0.5 m/s, the system demonstrates good stability, with a maximum error of 5.33%, indicating that the thrust is sufficient for maintaining the speed during horizontal movement. At 1 m/s, the current limitations again lead to significant increases in positional error, at a maximum of 23.33%, showing that the power demand at high speeds exceeds the available supply, affecting speed control accuracy.

Y-Direction Test: In the *Y*-direction test, with a target speed of 0.5 m/s, system performance is similar to that in the X-direction, with errors within ±5.33%, and a maximum of 5.33%. These results indicate that the system maintains stability in the *Y*-direction and effectively controls movement at low speeds.

Overall, the MDSMAC system effectively compensates for errors at low to medium speeds and quickly returns to the expected trajectory. At high speeds, current limitations reduce control precision, with significant error increases, particularly at 1 m/s.

4.3. Long-Term Operation Validation

4.3.1. Experiment Objective

The objective of this experiment is to verify the effectiveness of the MDSMAC algorithm during long-duration tasks and to evaluate the system's trajectory tracking accuracy and robustness over a 24 h period. By simulating an extended operational scenario, the experiment aims to analyze the system's stability and disturbance resistance over an extended timeframe.

4.3.2. Experimental Procedure

Fixed Trajectory Setup: In the experiment, the ROV was programmed to follow a straight path parallel to the main axis of the pool for a continuous 24 h period, focusing on assessing the intrinsic control stability of the system. The choice of a straight-line trajectory reflects a common and crucial motion pattern in cleaning tasks, providing a representative scenario, while facilitating precise measurement and analysis of trajectory deviations.

Data Recording and Monitoring: Throughout the experiment, the ROV's trajectory deviations and control input variations were recorded at regular intervals, focusing on the maximum deviations in the X, Y, and Z directions. Data collection points were set at the 1st, 3rd, 6th, 12th, 18th, and 24th hours to monitor system performance over time. These data points allow for the observation of trajectory deviation trends and the assessment of system stability and control input consistency throughout long-term operation.

4.3.3. Experimental Results

The experimental results are shown in Figure 12, which presents the maximum trajectory deviations over the 24 h operation period.

As seen in Figure 14, the deviations in the X-direction remained consistently close to zero, indicating that the ROV maintained stable motion along the wall, demonstrating high trajectory tracking accuracy on the horizontal axis. The maximum deviation in the X-direction was maintained within 0.02 m, further confirming the system's reliability and precise control during long-duration tasks. In the Y-direction, the deviations gradually increased over time, reaching 0.48 m at the 24 h mark, reflecting some cumulative error in the lateral direction. This accumulation could be attributed to the gradual buildup of minor deviations during prolonged operation. However, the system was still able to keep the trajectory within a controllable range, ensuring overall operational stability. The Z-direction deviations showed relative stability, ranging from 0.02 m to 0.06 m. This indicates that the system maintained robust performance in the vertical direction, demonstrating its capability to handle structural nonlinearities and internal disturbances effectively.

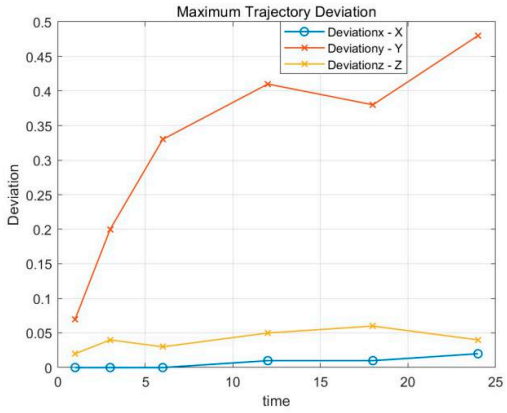

Figure 14. Maximum trajectory deviation.

These results validate the effectiveness of the MDSMAC algorithm for long-duration tasks, showcasing its strong performance in maintaining trajectory tracking accuracy and handling structural nonlinearities.

4.4. Analysis and Discussion

4.4.1. Gaussian Assumption and Robustness of MDSMAC

This study explores the application of the Gaussian assumption in control systems, validating its effectiveness in modeling external disturbances, particularly in capturing the randomness and uncertainty inherent in natural disturbances. Both the simulation and experimental results demonstrate that the Gaussian distribution significantly enhances system stability and control accuracy, especially when dealing with Gaussian-type disturbances. The MDSMAC algorithm exhibits remarkable robustness in real-world conditions, effectively maintaining stable trajectory tracking, despite sensor drift and fluid dynamics. The Gaussian assumption provides strong theoretical support for control systems and improves the system's performance in complex environments, ensuring the stability and precision of the ROV in varying operational conditions.

4.4.2. Control Algorithm Comparison

The MDSMAC algorithm was compared with other common control strategies, revealing significant advantages in terms of accuracy, response speed, and system stability. Compared to traditional control methods, MDSMAC demonstrated superior robustness in handling structural nonlinearities and external disturbances, particularly in maintaining high-precision trajectory tracking during long-term operations. The simulation and experimental data further validate MDSMAC's stability in complex environments, with minimal error accumulation during high-speed and extended operations. In contrast, other control algorithms exhibited greater error accumulation and lower stability when dealing with the impacts of fluid dynamics and sensor inaccuracies. Overall, MDSMAC not only offers higher precision and a faster response, but also demonstrates superior stability, making it a reliable solution for automation in regard to complex tasks.

4.4.3. Analysis of Systematic Errors and Influencing Factors

The main factors affecting trajectory deviation during the experiment include the system's nonlinear characteristics, sensor measurement accuracy, sensor drift, and measurement errors.

Nonlinear characteristics of the physical system: Although the MDSMAC algorithm has strong disturbance rejection capabilities, the system is still influenced by practical physical factors, such as inertia and fluid resistance, which increase the deviation when

dealing with complex movements and nonlinear systems. Particularly in the Y-direction, the robot is more prone to lateral drift due to inertia and fluid dynamics during movement, exacerbating cumulative errors.

Sensor drift and measurement errors: Sensor drift is one of the main causes of error accumulation during long-term operation. In both the Y and Z directions, sensor drift causes the system to misinterpret its current position, gradually deviating from the intended trajectory. Although MDSMAC has adaptive adjustment functions that can counteract some drift errors, error accumulation remains inevitable in long-term continuous operation. The IMU's accelerometer range was adjusted to ± 2 g, with a sensitivity of 16,384 LSB/g, and the gyroscope range was set to ± 2000 dps, with a sensitivity of 16.4 LSB/$^\circ$/s. The depth sensor can measure depths up to 100 m, with an accuracy of 0.1 m. These sensor specifications influence the overall measurement accuracy and error dynamics.

Possible underestimation of error: One reason for the smaller deviation in the X-direction could be insufficient sensor resolution or accuracy, which may not detect very small displacements, leading to an underestimation of the actual error. Additionally, in the X-direction experiment, since the robot was closely following the wall, the measurement of the deviation might not have been as pronounced as in the Y and Z directions, making the accuracy in the X-direction seem overly optimistic.

Measurement errors and environmental factors: Water disturbances, irregularities in the wall surface, and sensor calibration errors in the experimental environment could all affect the accuracy of trajectory deviations. Even in a still water tank, minor disturbances may accumulate over time, contributing to larger errors.

Tolerance statement: In this study, we conducted a detailed analysis of the position measurement system's error tolerance. The system is designed to tolerate a maximum measurement error of ± 0.1 m, ensuring that the underwater robot maintains good trajectory tracking performance and system stability, even in the presence of measurement inaccuracies. By optimizing sensor placement and refining the control algorithm, the system effectively mitigates external disturbances and internal parameter uncertainties within the allowable error range, thereby enhancing the overall robustness and reliability of the MDSMAC strategy.

The experimental results show that MDSMAC achieves very high trajectory tracking accuracy in the X-direction during wall-following movements, which is crucial for operations in confined spaces, such as aquaculture tanks, highlighting the system's robustness in the face of environmental variations.

5. Conclusions and Future Research Directions

This study introduces an innovative multi-scale dynamic sliding mode adaptive control strategy designed to address the challenges encountered in underwater aquaculture cleaning tasks. These challenges include structural nonlinearities, parameter uncertainties, external environmental disturbances, and strong operational disturbances. Using comprehensive theoretical derivations, stability analyses, numerical simulations, and physical experiments, we have validated the effectiveness and robustness of the MDSMAC strategy in complex underwater environments.

The MDSMAC strategy significantly outperforms traditional control methods, such as PID control, FLC, SMC, and NNC, in terms of trajectory tracking accuracy and system stability, particularly when dealing with complex disturbances and nonlinear systems. The experimental results demonstrate that MDSMAC can achieve rapid trajectory tracking within 0.1 s, with mean square errors of 0.205, 0.063, and 0.008 in the X, Y, and Z directions, respectively. These values are substantially lower than those of other intelligent control

algorithms. Additionally, the absolute errors of 0.269, 0.239, and 0.087 further confirm the superior performance of MDSMAC in dynamic underwater environments.

Despite these advancements, there are areas for further improvement. The current simulation and experimental setups, while accounting for external disturbances, still have limitations in terms of simulation complexity and randomness, which do not fully capture all potential variations present in real-world environments. Future research should focus on testing the MDSMAC strategy in more complex and dynamic real-world settings to better simulate and address the uncertain disturbances encountered during actual operations. Furthermore, integrating advanced machine learning techniques, particularly adaptive parameter adjustment algorithms, can enhance the system's accuracy, adaptability, and responsiveness in different operating environments, especially in non-static underwater conditions. This integration will further improve the performance and robustness of MDSMAC in regard to complex tasks.

In summary, the MDSMAC strategy not only effectively manages multi-scale disturbances in underwater environments, but also overcomes the limitations of traditional control methods in handling complex nonlinear systems and external disturbances. Its key advantage lies in its ability to adapt to dynamically changing operating conditions, while achieving superior trajectory tracking accuracy and system stability. Its key advantage lies in its ability to adapt to dynamically changing operating conditions, while maintaining high trajectory tracking accuracy and system stability. Consequently, MDSMAC offers a more efficient and reliable control solution for underwater robotic systems, particularly in tasks such as underwater aquaculture cleaning. With continued research, MDSMAC is expected to demonstrate its potential across a broader range of application scenarios, especially in complex, dynamic, and uncertain environments, thereby enhancing system adaptability and control performance.

Overall, MDSMAC not only successfully addresses the limitations of traditional control methods in regard to specific applications, but also provides innovative solutions and practical approaches to similar complex control challenges. Therefore, this strategy has significant application potential in the field of underwater operations and offers valuable insights and references for nonlinear system control problems in other domains, showcasing strong scalability and broad applicability.

Author Contributions: Software, H.Z.; Formal analysis, H.Z.; Writing—original draft, H.Z.; Supervision, S.X. and Y.X.; Project administration, Y.X.; Funding acquisition, Y.X. All authors have read and agreed to the published version of the manuscript.

Funding: This study was financially supported by the "Pioneer" and "Leading Goose" R&D Program of Zhejiang (2022C03023).

Institutional Review Board Statement: Not applicable.

Informed Consent Statement: Not applicable.

Data Availability Statement: All data supporting the reported results are contained within the article.

Conflicts of Interest: The authors declare no conflict of interest.

References

1. FAO. The State of World Fisheries and Aquaculture. 2024. Available online: https://openknowledge.fao.org/items/b075d6b7-6c76-4a7e-9c6d-3b0ca36730fc (accessed on 1 June 2024).
2. Yuan, T.P.; Huang, X.H.; Hu, Y.; Wang, S.M.; Tao, Q.Y.; Pang, G.L. Aquaculture net cleaning with cavitation improves biofouling removal. *Ocean Eng.* **2023**, *285 Pt 1*, 115241. [CrossRef]
3. Fossen, T.I. *Handbook of Marine Craft Hydrodynamics and Motion Control*; John Wiley & Sons Inc.: Hoboken, NJ, USA, 2011; ISBN 9781119991496. [CrossRef]

4. Lekkas, A.M.; Fossen, T.I. Trajectory Tracking and Ocean Current Estimation for Marine Underactuated Vehicles. In Proceedings of the 2014 IEEE Conference on Control Applications (CCA), Juan Les Antibes, France, 8–10 October 2014; pp. 905–910. [CrossRef]
5. Bayusari, A.M.; Alfarino, H.; Husin, Z.; Dwijayanti, S.; Suprapto, B.Y. Position Control System of Autonomous Underwater Vehicle using PID Controller. In Proceedings of the 2021 8th International Conference on Electrical Engineering, Computer Science and Informatics (EECSI), Semarang, Indonesia, 20–21 October 2021; pp. 139–143. [CrossRef]
6. Bhattacharya, D.; Puttamadappa, C. PID-Fuzzy Control System for Autonomous Underwater Vehicles (AUV): Highly Accurate FPGA Implementation. *Philipp. J. Sci.* **2023**, *152*, 20. [CrossRef]
7. Zhang, Z.; Wu, Y. Adaptive Fuzzy Tracking Control of Autonomous Underwater Vehicles with Output Constraints. *IEEE Trans. Fuzzy Syst.* **2021**, *29*, 1311–1319. [CrossRef]
8. Tabar, A.F.; Azadi, M.; Alesaadi, A. Sliding Mode Control of Autonomous Underwater Vehicles. *Int. J. Electr. Comput. Eng.* **2015**, *8*, 546–549.
9. Minh, V.; Moezzi, R.; Dhoska, K.; Pumwa, J. Model Predictive Control for Autonomous Vehicle Tracking. *Int. J. Innov. Technol. Interdiscip. Sci.* **2021**, *4*, 560–603. [CrossRef]
10. Gomes, R.; Pereira, F.L. Model Predictive Control for Autonomous Underwater Vehicles. *Procedia Comput. Sci.* **2019**, *150*, 19–27. [CrossRef]
11. Amin, R.; Khayyat, A.A.; Osgouie, K.G. Neural networks control of autonomous underwater vehicle. In Proceedings of the 2010 2nd International Conference on Mechanical and Electronics Engineering, Kyoto, Japan, 1–3 August 2010; pp. V2-117–V2-121. [CrossRef]
12. Elhaki, O.; Shojaei, K. Neural network-based target tracking control of underactuated autonomous underwater vehicles with a prescribed performance. *Ocean Eng.* **2018**, *167*, 239–256. [CrossRef]
13. Shen, C.; Shi, Y.; Buckham, B. Trajectory Tracking Control of an Autonomous Underwater Vehicle Using Lyapunov-Based Model Predictive Control. *IEEE Trans. Ind. Electron.* **2018**, *65*, 5796–5805. [CrossRef]
14. Yang, M.; Sheng, Z.; Yin, G.; Wang, H. A Recurrent Neural Network-Based Fuzzy Sliding Mode Control for 4-DOF ROV Movements. *Ocean Eng.* **2022**, *256*, 111509. [CrossRef]
15. Long, C.; Qin, X.; Bian, Y.; Hu, M. Trajectory Tracking Control of ROVs Considering External Disturbances and Measurement Noises Using ESKF-Based MPC. *Ocean Eng.* **2021**, *241*, 109991. [CrossRef]
16. Zhang, X.; Zhou, H.; Fu, J.; Wen, H.; Yao, B.; Lian, L. Adaptive Integral Terminal Sliding Mode Based Trajectory Tracking Control of Underwater Glider. *Ocean Eng.* **2023**, *269*, 113436. [CrossRef]
17. Chen, H.; Tang, G.; Huang, Y.; Wang, J.; Huang, H. Adaptive Model-Parameter-Free Nonsingular Fixed-Time Sliding Mode Control for Underwater Cleaning Vehicle. *Ocean Eng.* **2022**, *262*, 112239. [CrossRef]
18. Liu, T.; Zhao, J.; Huang, J. A Gaussian-Process-Based Model Predictive Control Approach for Trajectory Tracking and Obstacle Avoidance in Autonomous Underwater Vehicles. *J. Mar. Sci. Eng.* **2024**, *12*, 676. [CrossRef]
19. Mei, L.; Chen, H.; Yang, X.; Gui, F. Statistical Properties of Extreme Waves in Multidirectional Wave Fields Over a Sloping Bottom. *Ocean Dyn.* **2023**, *1*, 1–23.
20. Chen, H.; Zhao, Y.; Mei, L.; Gui, F. Laboratory Observation of Nonlinear Wave Shapes Due to Spatial Varying Opposing Currents. *Coast. Eng.* **2024**, *190*, 104500. [CrossRef]
21. Chen, H.; Tang, X.; Gao, J.; Fan, G. Parameterization of Geometric Characteristics for Extreme Waves in Shallow Water. *Ocean Eng.* **2018**, *156*, 61–71. [CrossRef]
22. Liu, Z.; Zhang, O.; Gao, Y.; Zhao, Y.; Sun, Y.; Liu, J. Adaptive Neural Network-Based Fixed-Time Control for Trajectory Tracking of Robotic Systems. *IEEE Trans. Circuits Syst. II Express Briefs* **2023**, *70*, 241–245. [CrossRef]
23. Wang, J.-S.; Yuan, Y.-F.; Xie, F. Numerical Simulation of Cavitation Jet of Novel Series Combined Nozzles. *Min. Mach.* **2022**, *11*, 57–61.
24. Wei, H.; Huang, C. Innovative Design of Crawling Robot. *Dev. Innov. Mech. Electr. Prod.* **2018**, *31*, 11–13.
25. Kong, W. Study on Design and Motion Performance of Magnetic Track Underwater Cleaning Robot. Master's Thesis, Jiangsu University of Science and Technology, Jiangsu, China, 2021.
26. Yu, H.; Xu, Y.; Wang, J.; Liu, H.; Zhang, J.; Wang, Z. Numerical Simulation of Cavitation Jet Characteristics of Organ Pipe Nozzles. *Contemp. Chem. Ind.* **2022**, *51*, 1991–1995.